ANL-12/31

Scoping Analysis of the Advanced Test Reactor Using SN2ND

Nuclear Engineering Division

About Argonne National Laboratory
Argonne is a U.S. Department of Energy laboratory managed by UChicago Argonne, LLC under contract DE-AC02-06CH11357. The Laboratory's main facility is outside Chicago, at 9700 South Cass Avenue, Argonne, Illinois 60439. For information about Argonne, see www.anl.gov.

Availability of This Report
This report is available, at no cost, at http://www.osti.gov/bridge. It is also available on paper to the U.S. Department of Energy and its contractors, for a processing fee, from:

U.S. Department of Energy
Office of Scientific and Technical Information
P.O. Box 62
Oak Ridge, TN 37831-0062
phone (865) 576-8401
fax (865) 576-5728
reports@adonis.osti.gov

Disclaimer
This report was prepared as an account of work sponsored by an agency of the United States Government. Neither the United States Government nor any agency thereof, nor UChicago Argonne, LLC, nor any of their employees or officers, makes any warranty, express or implied, or assumes any legal liability or responsibility for the accuracy, completeness, or usefulness of any information, apparatus, product, or process disclosed, or represents that its use would not infringe privately owned rights. Reference herein to any specific commercial product, process, or service by trade name, trademark, manufacturer, or otherwise, does not necessarily constitute or imply its endorsement, recommendation, or favoring by the United States Government or any agency thereof. The views and opinions of document authors expressed herein do not necessarily state or reflect those of the United States Government or any agency thereof, Argonne National Laboratory, or UChicago Argonne, LLC.

ANL-12/31

Scoping Analysis of the Advanced Test Reactor Using SN2ND

by E. Wolters, M.A. Smith
Nuclear Engineering Division, Argonne National Laboratory

June 30, 2012

EXECUTIVE SUMMARY

A detailed set of calculations was carried out for the Advanced Test Reactor (ATR) using the SN2ND solver of the UNIC code which is part of the SHARP multi-physics code being developed under the Nuclear Energy Advanced Modeling and Simulation (NEAMS) program in DOE-NE. The primary motivation of this work is to assess whether high fidelity deterministic transport codes can tackle coupled dynamics simulations of the ATR. The successful use of such codes in a coupled dynamics simulation can impact what experiments are performed and what power levels are permitted during those experiments at the ATR.

The advantages of the SN2ND solver over comparable neutronics tools are its superior parallel performance and demonstrated accuracy on large scale homogeneous and heterogeneous reactor geometries. However, it should be noted that virtually no effort from this project was spent constructing a proper cross section generation methodology for the ATR usable in the SN2ND solver. While attempts were made to use cross section data derived from SCALE, the minimal number of compositional cross section sets were generated to be consistent with the reference Monte Carlo input specification. The accuracy of any deterministic transport solver is impacted by such an approach and clearly it causes substantial errors in this work. The reasoning behind this decision is justified given the overall funding dedicated to the task (two months) and the real focus of the work: can modern deterministic tools actually treat complex facilities like the ATR with heterogeneous geometry modeling.

SN2ND has been demonstrated to solve problems with upwards of one trillion degrees of freedom which translates to tens of millions of finite elements, hundreds of angles, and hundreds of energy groups, resulting in a very high-fidelity model of the system unachievable by most deterministic transport codes today. A space-angle convergence study was conducted to determine the meshing and angular cubature requirements for the ATR, and also to demonstrate the feasibility of performing this analysis with a deterministic transport code capable of modeling heterogeneous geometries. The work performed indicates that a minimum of 260,000 linear finite elements combined with a L3T11 cubature (96 angles on the sphere) is required for both eigenvalue and flux convergence of the ATR. A critical finding was that the fuel meat and water channels must each be meshed with at least 3 “radial zones” for accurate flux convergence. A small number of 3D calculations were also performed to show axial mesh and eigenvalue convergence for a full core problem. Finally, a brief analysis was performed with different cross sections sets generated from DRAGON and SCALE, and the findings show that more effort will be required to improve the multi-group cross section generation process.

The total number of degrees of freedom for a converged 27 group, 2D ATR problem is ~340 million. This number increases to ~25 billion for a 3D ATR problem. This scoping study shows that both 2D and 3D calculations are well within the capabilities of the current SN2ND solver, given the availability of a large-scale computing center such as BlueGene/P. However, dynamics calculations are not realistic without the implementation of improvements in the solver.

INTRODUCTION

A detailed set of calculations was carried out for the Advanced Test Reactor (ATR) [1] using the SN2ND solver of the UNIC code [2] which is part of the SHARP multi-physics code [3] being developed under the Nuclear Energy Advanced Modeling and Simulation (NEAMS) program in DOE-NE. The primary motivation of this work is to assess whether high fidelity deterministic transport codes can treat coupled dynamics simulations of the ATR. The successful use of such codes in a coupled dynamics simulation can impact what experiments are performed and what power levels are permitted during those experiments at ATR. The advantages of the SN2ND solver over comparable neutronics tools are its superior parallel performance [4-5] and demonstrated accuracy on large scale homogeneous and heterogeneous reactor geometries [6-7].

To date, we have found that the accuracy of the SN2ND solver has been limited by the multi-group cross section generation procedure, and we have similar concerns for the ATR. While the methodologies for heterogeneous cross section generation in thermal reactor systems are more mature than the fast reactors we have considered thus far [6-7], we still estimate that it will take 2-4 months of effort just to look into the issue for the ATR. We also note that the sub-group methodology is likely the preferred approach in the long term for a dynamics calculation, but there is (likely) no sub-group library (or procedure for generating one) available for the ATR today due to the rather complex nature of the problem.

Given the poor accuracy of the eigenvalue results appearing in this report, the preceding concerns are justified, but understandable given the limited funding for this task (two months). Consequently, we **ignore** the importance of the eigenvalue accuracy in this work and only focus on the fundamental problem size issue associated with the heterogeneous modeling of any such facility. Such an approach is valid given the uncertainty about whether the ATR can even be solved heterogeneously at this time with deterministic transport solvers. We strongly suggest cross section generation as future work as deemed necessary by the parties that are interested in this work.

There are only a few deterministic transport codes that can treat the explicit geometry, and of those, not many can go beyond a few billion degrees of freedom with a reasonable amount of computing time. That translates to a few million finite elements, a few hundred angles, and tens of groups ($10^6*10^2*10^1=10^9$). Using SN2ND on a super-computer like BlueGene/P [8], that number can be pushed to one trillion degrees of freedom which translates to tens of millions of finite elements, hundreds of angles, and hundreds of groups ($10^7*10^2*10^2=\sim10^{11}$). The largest problem we have ever executed using SN2ND contained ~0.5 trillion degrees of freedom.

In the case of ATR, the goal is to determine the necessary mesh and angle refinement required to resolve the spatial gradients. While we did test several energy structures to ensure that the chosen cross section data would be consistent with a rigorous multi-group cross section procedure, a full assessment of error due to the number of energy groups is left for future work. Because of the design of the ATR (control rods are not inserted axially, but rotated into position), a bulk of the analysis

can be carried out using two-dimensional geometries. Several two-dimensional meshes were constructed and combined with various angular cubatures such that detailed point-wise flux gradients can be displayed to show convergence. As expected, significant mesh refinement is required to obtain spatial convergence, particularly near the fuel plates and the water channels that surround them. Given that time on the supercomputer is not free, a few selected calculations on a three-dimensional geometry were carried out to determine the three-dimensional mesh refinement needs and get a sense of the overall computational expense.

DISCUSSION

Steady state reactor analysis involves three essential discretizations: (1) selection and generation of appropriate multigroup constants, (2) determination of an appropriate spatial mesh, and (3) determination of an appropriate angular discretization. The aim of this report is to assess and make a recommendation on the discretizations required in space and angle for the Advanced Test Reactor (ATR). Spatial and angular discretization requirements are first examined in 2D using several finite element meshes combined with different angular cubatures. Only a few detailed 3D calculations were performed using the settings from the 2D convergence studies which is valid for the ATR because of the way the reactor system is designed (control rods are not inserted axially, but radially rotated into position).

For completeness, a brief study is performed on the dependence on different energy group structures in addition to the importance of anisotropic scattering. Unless otherwise stated, all calculations are performed using a 23 group cross section set (isotopic) generated via DRAGON [9]. DRAGON was chosen to generate multigroup cross sections because of its accessibility and ease of use (it outputs data in the ISOTXS format usable by UNIC). We note that the sub-group library we used in DRAGON is not valid for the highly enriched U-235 compositions of the ATR fuel nor is the lattice geometry model we used (slab) very appropriate. As a consequence, the DRAGON multigroup constants used in this work can at best be considered representative. In addition to DRAGON, we obtained the SCALE [10] cross section generation procedure created by Idaho National Laboratory for the ATR and used SCALE to generate 23 group, 27 group, and 49 group cross section sets. More time must be invested in implementing an alternative cross section generation procedure before attempting any detailed dynamics calculation.

1.1 Specification of 2D Finite Element Meshes

Several unstructured, conformal, 2D finite element meshes (labeled Mesh A-E) were generated for the ATR using the CUBIT mesh generation toolkit [11]. Because of the small element sizes that are required to model the ATR's complex geometry, there is no need to use high order basis functions in SN2ND. Thus linear finite elements were specified for all meshes where the volume fractions of each region are rigorously preserved on each mesh. It should be noted that SN2ND can use the higher order basis

elements, but at a considerable computational cost due to the element aspect ratios that come naturally with meshing the ATR.

To avoid very poor aspect ratios, a mix of triangles and quadrilaterals (prisms and hexahedrons in 3D) are used to facilitate the meshing of the ATR. While quadrilateral finite elements are generally preferred for spatial mesh convergence, triangular finite elements are more flexible and were required to coarsely mesh some of the more complex geometric components (particularly the measurement zones). Additionally, triangular finite elements were strategically used to transition from coarser to finer meshes, as dictated by the local geometrical complexity.

Five particular 2D meshes are described here in order of increasing refinement. We point out the progressive changes made to each mesh and give the total number of vertices and finite elements. Table 1 gives the overall summary in mesh vertices and finite elements for quick reference.

Mesh A: Mesh A is the coarsest possible mesh we were able to generate which can represent the ATR geometry. Figure 1 shows an overall view of the mesh focused on the active core while Figure 2 shows a close-up view of the mesh in the fuel bundle near the inner measurement zone in the right lobe. Figure 3 shows a close-up view of the mesh for the control rod drums. Mesh A has a total of 61,797 vertices and 66,073 finite elements where the following important factors are of note:

- The fuel meat in each fuel plate (nineteen plates per fuel section) and the water channels between fuel plates were subdivided lengthwise into 8 quadrilateral elements and not subdivided radially (see Figure 2).
- The Hafnium material in the control barrel drums was partitioned into 31 triangular elements (see Figure 3).
- The Hafnium material in the neck shim rods was subdivided into 8 annular intervals, each approximated by a quadrilateral (see Figure 2).

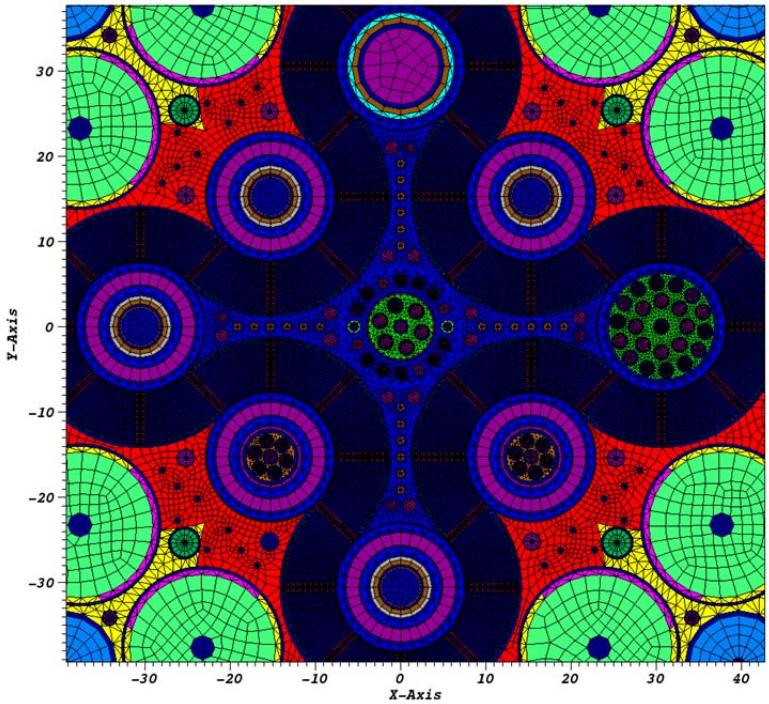

Figure 1. Mesh A, Overall View of the ATR Active Core.

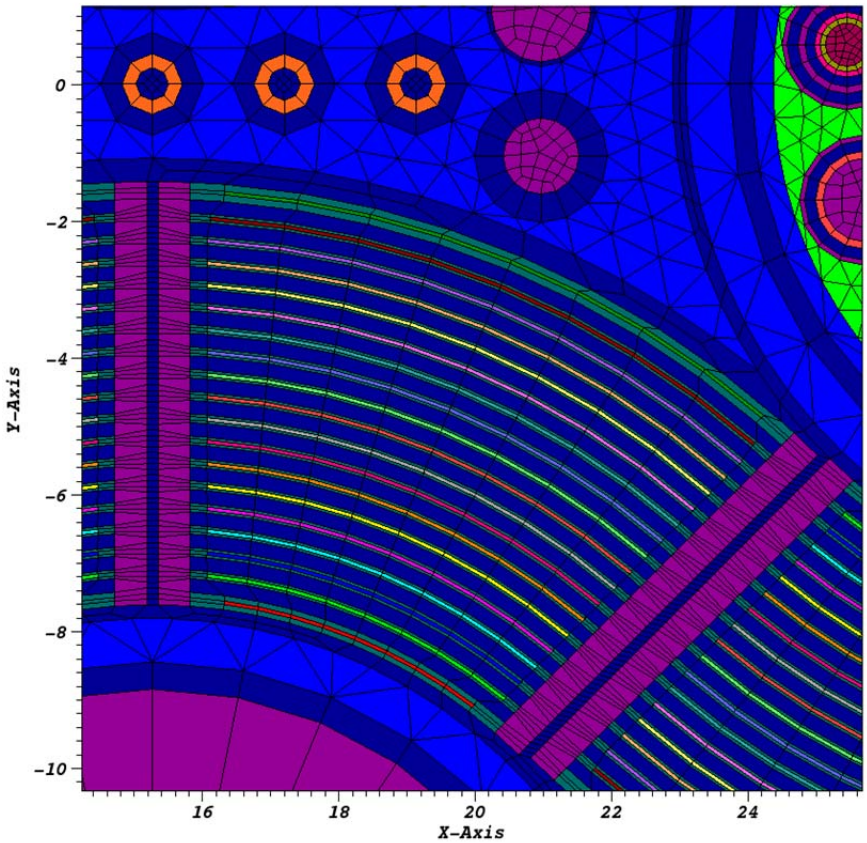

Figure 2. Mesh A, Close-up View of a Fuel Bundle and Neck Hafnium Shim Rods.

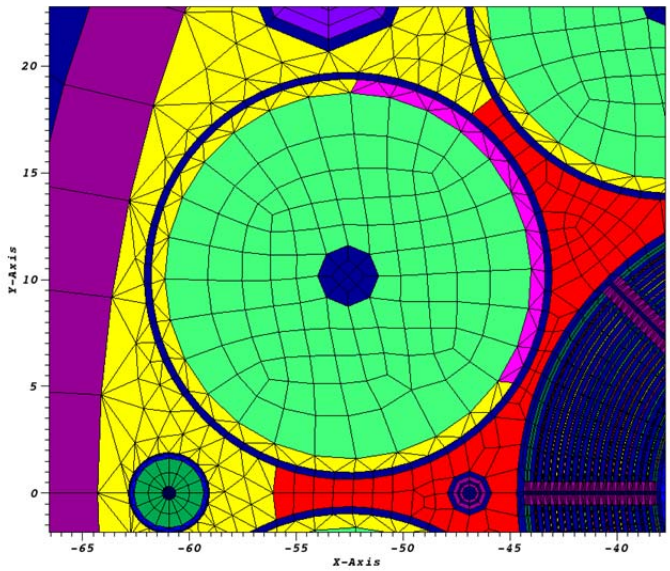

Figure 3. Mesh A, Outer Control Barrel (Hafnium is Partial Magenta Ring).

Mesh B: Mesh refinement was focused on the fuel meat and hafnium regions. These targeted refinements also resulted in unavoidable refinements of neighboring materials to keep the mesh conformal. Figure 4 can be compared with the Mesh A result in Figure 2. Mesh B has a total of 121,431 vertices and 128,409 finite elements where the following important choices were made to Mesh A.

- The fuel meat and adjacent water channels in each fuel bundle was divided lengthwise into 24 segments.
- The hafnium material in the annulus of the neck shim rods was divided into 12 annular intervals and 2 radial intervals for a total of 24 quadrilateral elements.
- The Hafnium component of the control barrel was partitioned into 63 triangular elements (about twice as many as before).

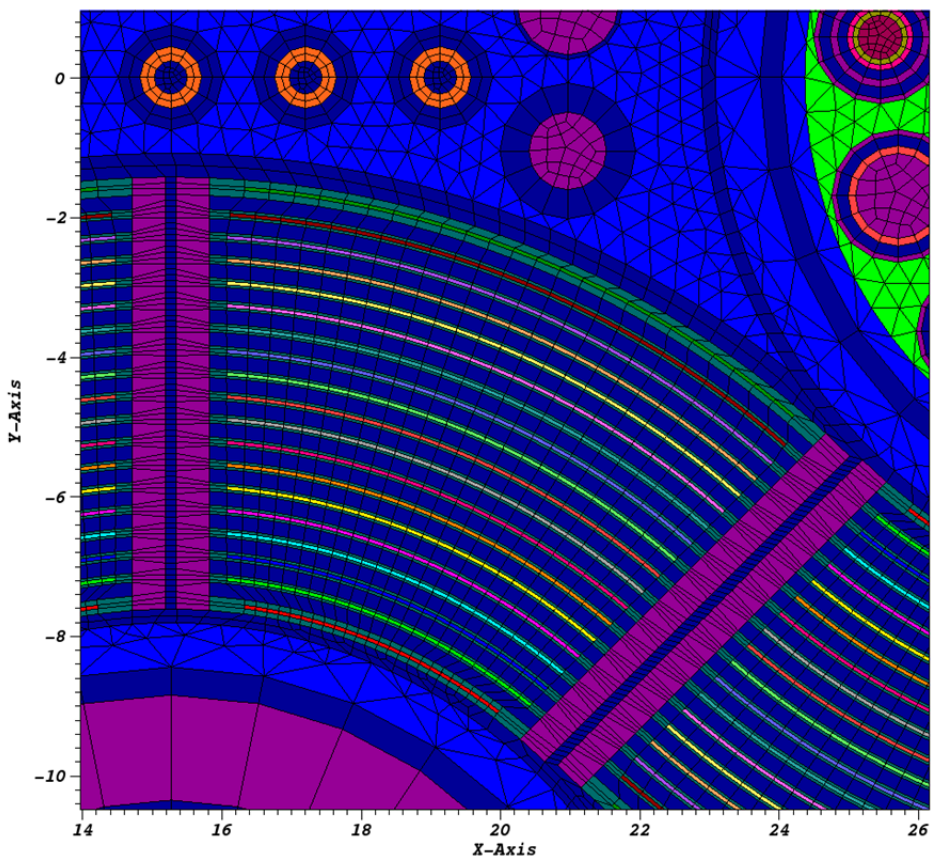

Figure 4. Mesh B, Close-up View of a Fuel Bundle and Neck Hafnium Shim Rods.

Mesh C: The fuel meat was refined "radially" into 3 elements from Mesh B, and the refinements to the Hafnium regions made in Mesh B were maintained. Figure 5 shows the radial refinement of the fuel meat where Mesh B only has a single finite element across the same region. Mesh C has a total of 183,994 vertices and 190,972 finite elements with the following notable choices:

- The fuel meat in each fuel plate was divided lengthwise into 24 elements and widthwise into 3 elements.
- The water channels between fuel plates were divided lengthwise into 24 elements, as in Mesh B.
- The refinement of the Hafnium material in the neck shim rods and control barrel is identical as that in Mesh B.

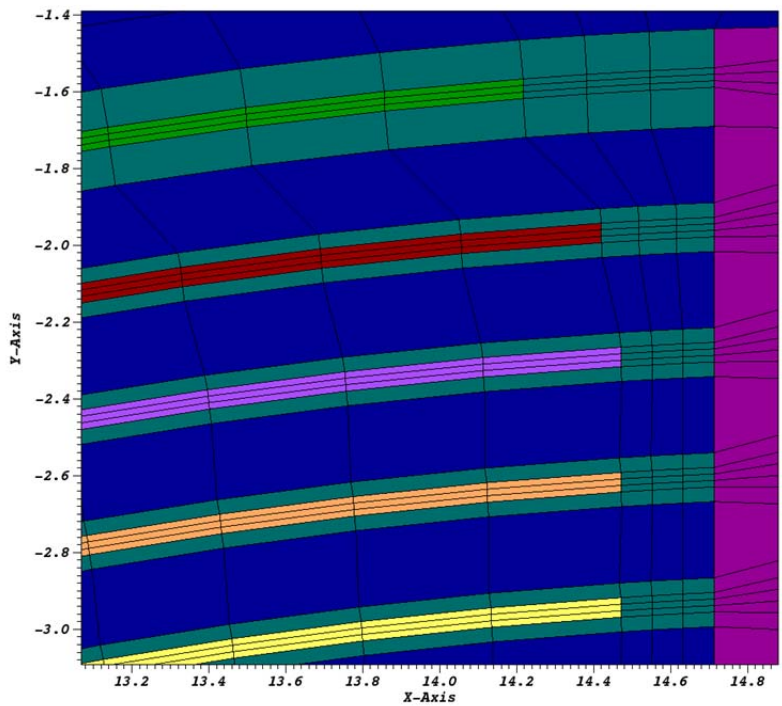

Figure 5. Mesh C, Extreme Close-up View of a Fuel Bundle.

Mesh D: The fuel meat and hafnium regions used the same mesh as in Mesh C. However, the water channels between fuel plates were radially refined from 24x1 to 24x3 elements as shown in Figure 6. Mesh D has a total of 256,005 vertices and 262,983 finite elements.

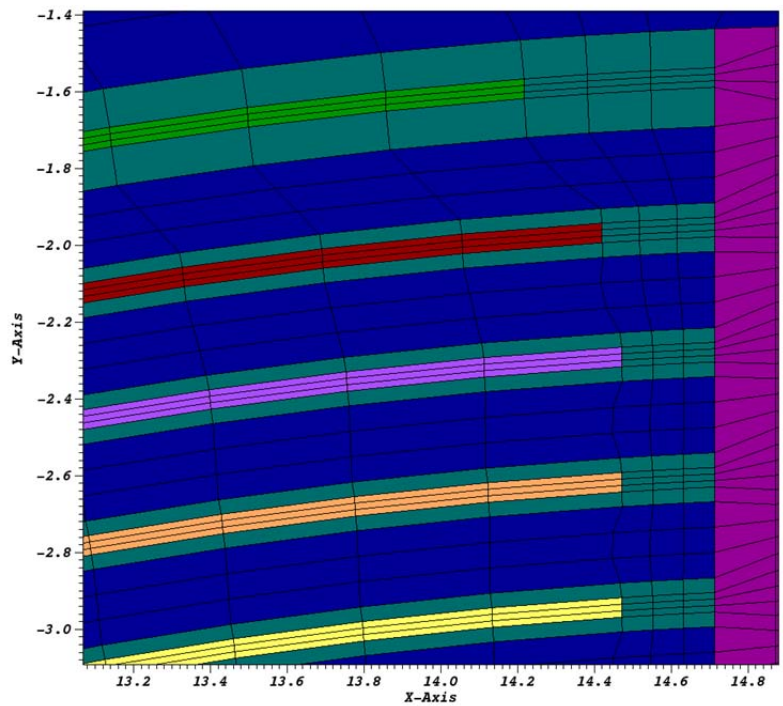

Figure 6. Mesh D, Extreme Close-up View of a Fuel Bundle.

Mesh E: The fuel meat, water between plates, and cladding were refined again lengthwise and radially as shown in Figure 7. Mesh E has a total of 788,930 vertices and 781,349 finite elements where the following changes were made:

- The fuel meat in each fuel plate was refined to 64x4 elements.
- The fuel plate cladding was refined to 64x2 elements.
- The water channels between fuel plates were divided into 64x4 elements, as opposed to 24x3 elements as in Mesh D.

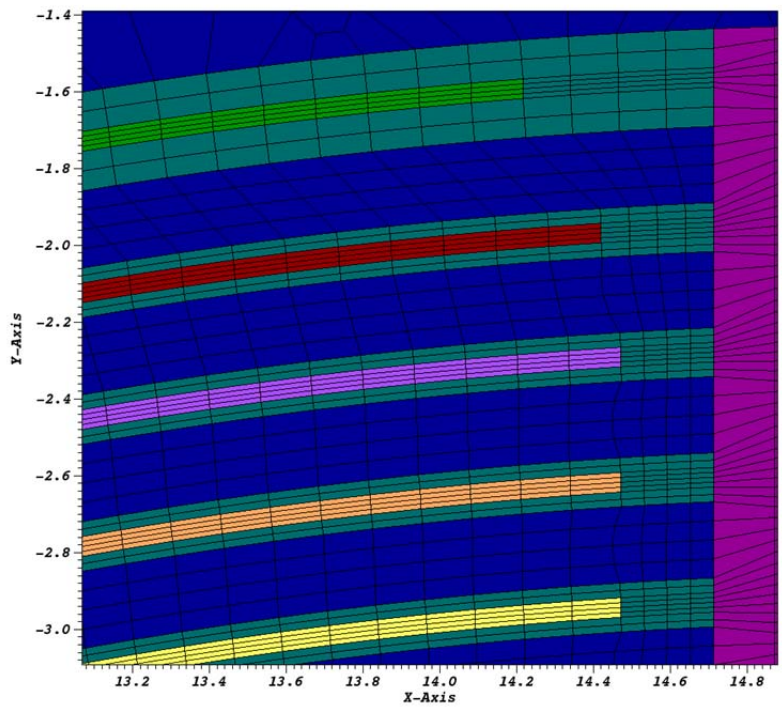

Figure 7. Mesh E, Extreme Close-up View of a Fuel Bundle.

Table 1. Summary of the Two-dimensional Finite Element Meshes.

Number of Elements	Mesh A	Mesh B	Mesh C	Mesh D	Mesh E
Total	66,073	128,409	190,972	262,983	781,349
Fuel Meat	8 (8x1)	24 (24x1)	72 (24x3)	72 (24x3)	256 (64x4)
Fuel Plate Cladding	8 (8x1)	24 (24x1)	24 (24x1)	24 (24x1)	128 (64x2)
Water Between Plates	8 (8x1)	24 (24x1)	24 (24x1)	72 (24x3)	256 (64x4)
Hafnium Control Rods	8 (8x1)	24 (12x2)	24 (12x2)	24 (12x2)	24 (12x2)
Hafnium in Control Barrel	31	63	63	63	63

1.2 Assessment of Spatial and Angular Convergence in 2D

The geometric detail of the ATR is contained primarily within the X-Y plane, therefore 2D calculations are a reasonable starting point to examine angular cubature requirements. Several angular cubatures were used with each mesh to determine the impact on the eigenvalue and on the flux convergence for the two specific lines shown in Figure 8. As can be seen, Line 1 passes through the SW flux trap and the NE Measurement region centers. Line 2 passes through fuel sections 29, 30, 1, and 2, as well as the outer control barrels. See reference [1] for detailed information on the ATR geometry.

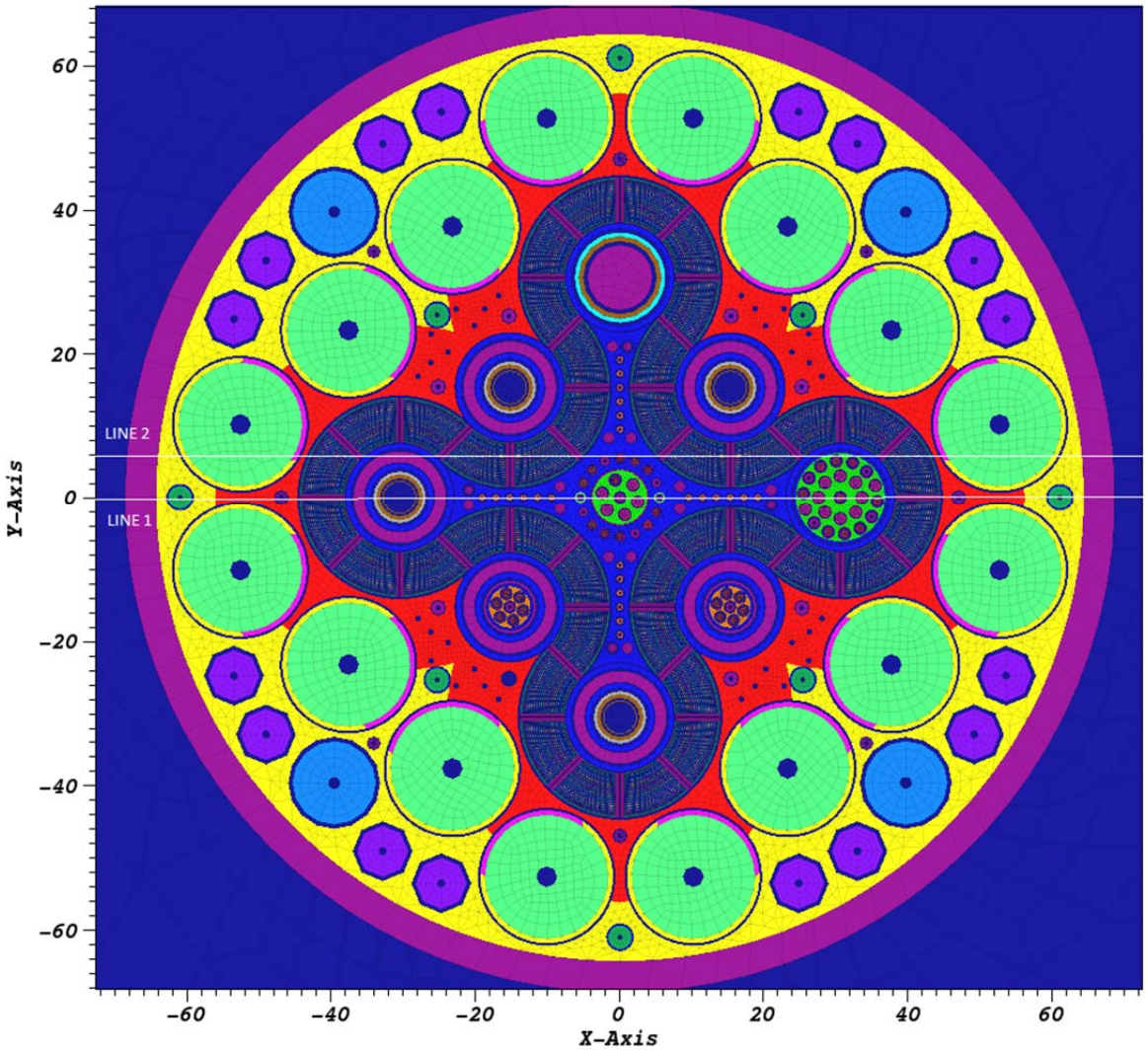

Figure 8. Illustration of the Two Lines Chosen to Analyze the Flux.

Table 2 summarizes the eigenvalues obtained with various angular approximations and spatial meshes. Note that the meshes are alphabetically ordered from coarsest (Mesh A) to finest (Mesh E). While other cubatures are available, the Legendre-Tchebychev product cubature was chosen because it allows the number of axial angular directions to be varied independently of the radial angular directions. The Legendre (L) order dictates the number of axial planes at which collections of Tchebychev angles are placed on the sphere as shown in Figure 9. Since the ATR geometry is complex in the X-Y direction, a high number of Tchebychev angles are required to achieve convergence.

The eigenvalue results are also plotted in Figure 10 with respect to the number of angles on the sphere which clearly shows the asymptotic convergence in both angle and mesh. From the eigenvalue results, angular convergence with respect to Tchebychev occurs near the T15 setting (15 pcm between L7T15 and L7T31 of Mesh E). Similarly,

angular convergence with respect to Legendre is near L7 as there is only 10 pcm error between L3T15 and L7T15. Additional plots are given later for more detailed consideration.

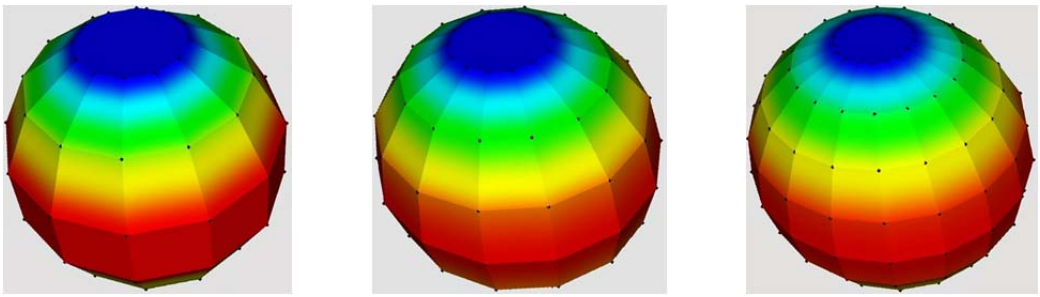

L5T9 L6T11 L7T15

Figure 9. Example Legendre-Tchebychev Product Cubatures.

Table 2. Eigenvalue Results for Various Angular Cubature and Spatial Meshes.

Angular Cubature	Angles on Unit Sphere	Mesh A	Mesh B	Mesh C	Mesh D	Mesh E
L1T1	8	1.04871	1.04912	1.04740	1.04463	1.04459
L3T3	32	1.05350	1.05394	1.05092	1.04794	1.04780
L3T7	64	1.05426	1.05458	1.05149	1.04900	1.04866
L3T15	128	1.05464	1.05529	1.05240	1.04970	1.04959
L3T31	256	1.05459	1.05518	1.05232	1.04961	1.04945
L7T3	64	1.05394	1.05439	1.05125	1.04807	1.04790
L7T7	128	1.05471	1.05499	1.05183	1.04911	1.04876
L7T15	256	1.05509	1.05576	1.05273	1.04983	1.04970
L7T31	512	1.05503	1.05564	1.05266	1.04973	1.04955

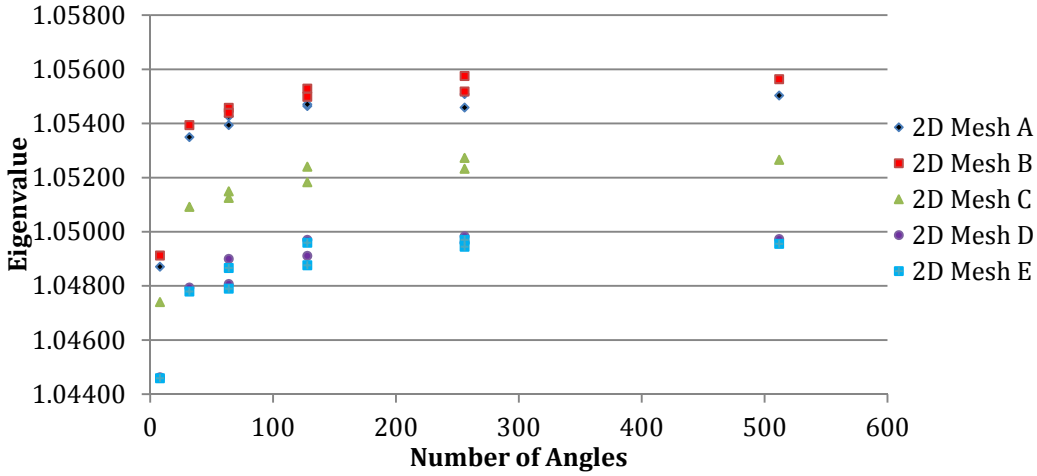

Figure 10. Angular and Spatial Convergence of Eigenvalues with 2D Meshes.

While angular convergence is similar between the meshes, an overall error of 600 pcm is observed in the eigenvalue due to mesh refinement. However, most of the error in the eigenvalue is removed between Mesh B and Mesh D, with little change in the eigenvalue between Mesh D and Mesh E. The 300 pcm drop in the eigenvalue from Mesh B to Mesh C is directly attributable to the subdivision of the fuel meat into 3 radial regions which indicates that detailed meshing in the fuel meat is essential to accurately converge the eigenvalue solution. Further, mesh refinement in the water channels is equally important, as evidenced by the nearly 300 pcm drop from Mesh C to Mesh D. Additional mesh refinement in those areas is of minor importance as indicated by the lack of change between Mesh D and Mesh E.

Taking the L7T15 cubature as the comparison point, two energy groups of the DRAGON 23 group structure were chosen to examine the flux convergence: Group 4 (111 – 500 keV) and Group 22 (0.05 – 0.1 eV). These energy groups represent the peak of the fission source (Group 4) and the peak of the thermal flux (Group 22) which should show the steepest gradients in the fuel bundle. The flux solutions along the two lines in Figure 8 are plotted in Figure 11 and Figure 13 for Group 4, and Figure 12 and Figure 14 for Group 22. To better show the flux convergence, a close-up of the flux distribution in the fuel bundle along Line 1 is shown in Figures 15-16. In all of the pictures, it is important to note that DRAGON did not provide fission rate conversion factors and thus the solutions are normalized incorrectly (i.e. not 10^{14}).

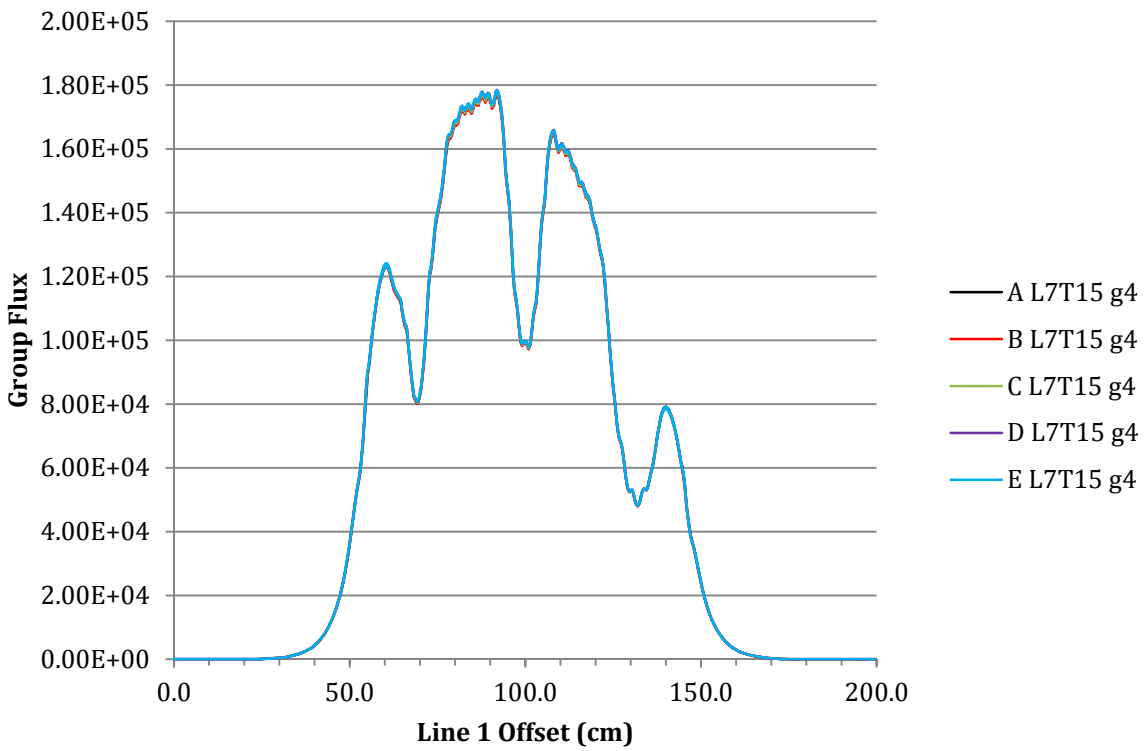

Figure 11. Fast Flux Solution (Group 4) Along Line 1 with Five Different Meshes.

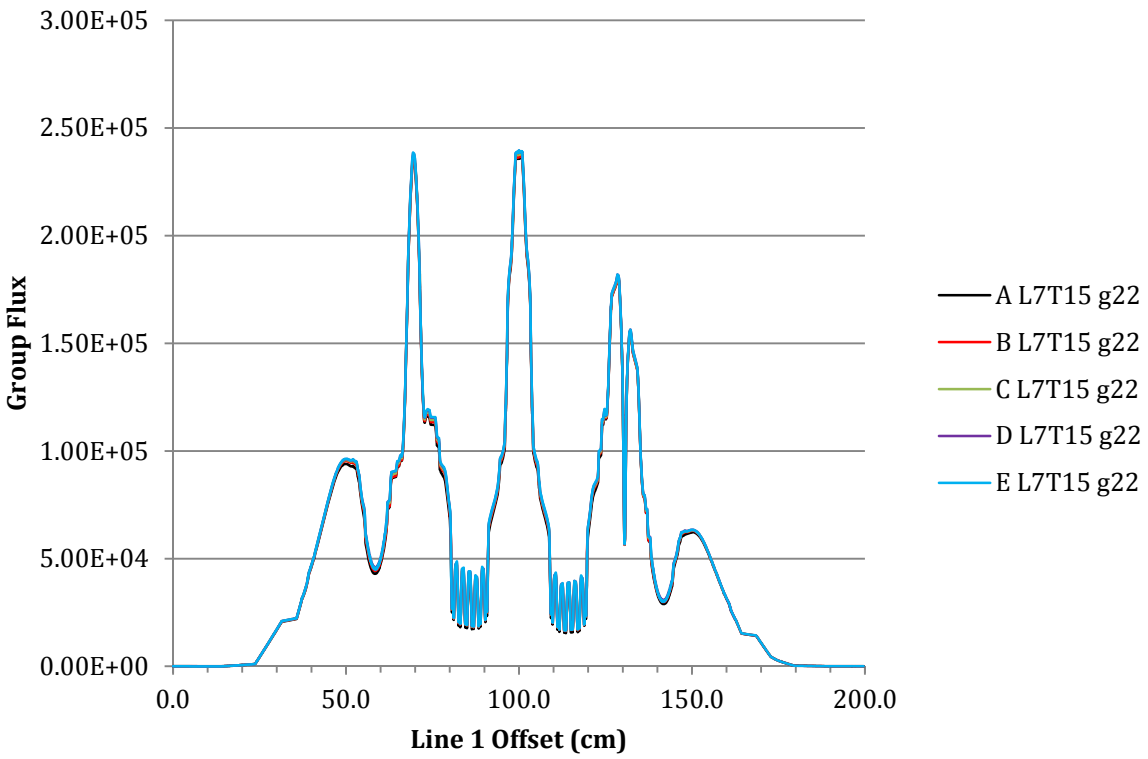

Figure 12. Thermal Flux Solution (Group 22) Along Line 1 with Five Different Meshes.

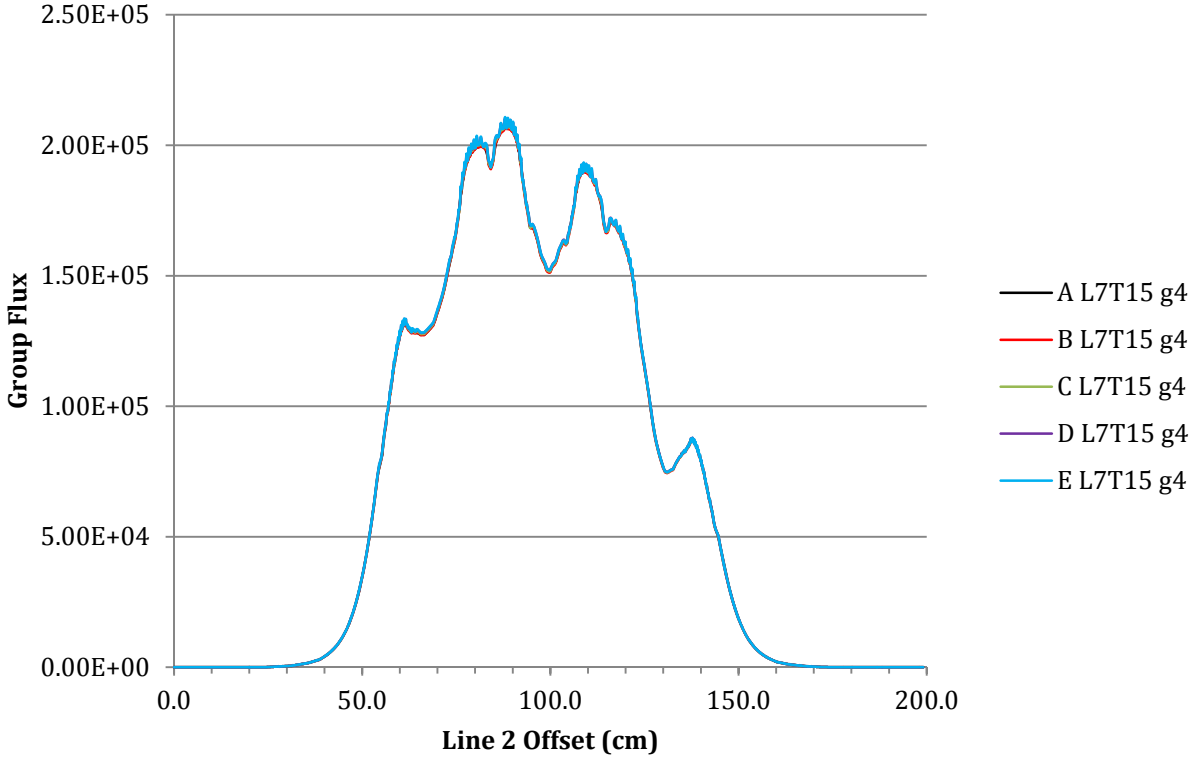

Figure 13. Fast Flux Solution (Group 4) Along Line 2 with Five Different Meshes.

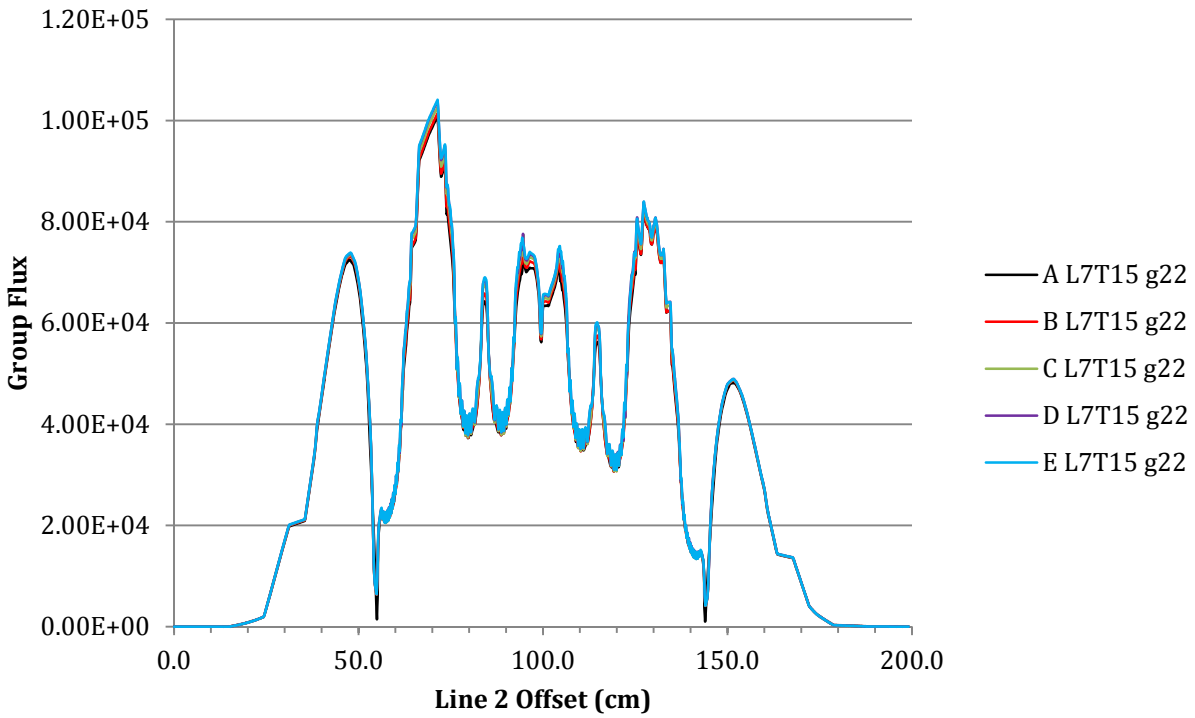

Figure 14. Thermal Flux Solution (Group 22) Along Line 2 with Five Different Meshes.

As can be seen in Figure 11 through Figure 14, there is considerable variation in the flux solution over the entire core. The Group 4 flux solution along Line 1 clearly shows the expected peak of the fast flux near the fuel bundles and on the narrow neck regions. Similarly, the Group 22 flux solution shows considerable thermal flux peaks in the lobe measurement zones and in the beryllium reflectors. One significant change to note between Line 1 and Line 2 is how the hafnium control drums cause very sharp drops in the thermal flux (Figure 14). Also note how pronounced the thermal flux peak is at the center of the core relative to the Line 2 transit. This indicates that more mesh refinement in the central measurement zone might be necessary to ensure accuracy in those regions. Note that additional angular refinement might also be necessary. Finally, the Line 1 plot clearly shows the importance of the hafnium shim rods in the neck shim area of the active core where rapid changes in the solution are observed. Improper meshing in these hafnium regions should cause an over-prediction in the absorption of neutrons. However, these errors are not as significant as the errors due to coarsely meshing the fuel plates and adjacent water channels.

Focusing on Figure 15 and Figure 16, one can clearly see the expected peaks in the fuel meat for the fast flux and peaks in the water channels for the thermal flux. Clearly the three coarsest meshes are inferior to the two finer meshes when it comes to describing such detail, and based upon the eigenvalue results, radial subdivision of the fuel meat and adjacent water channels is essential for the ATR. In both fast and thermal ranges, Meshes D and E have very similar flux distributions and it is therefore not surprising that the eigenvalue results were relatively insensitive to the additional mesh refinement.

With the preceding flux and eigenvalue results, we can conclude that further mesh refinement in the fuel bundles past Mesh D is not necessary for this steady state problem, although a dynamics simulation with widely varying temperature and density values might require something closer to Mesh E. We also note that some lengthwise refinement is required to maintain well-conditioned elements when using radial subdivision, and the current elements might not behave well in a coupled physics calculation involving thermal mechanics (i.e. might need further refinement).

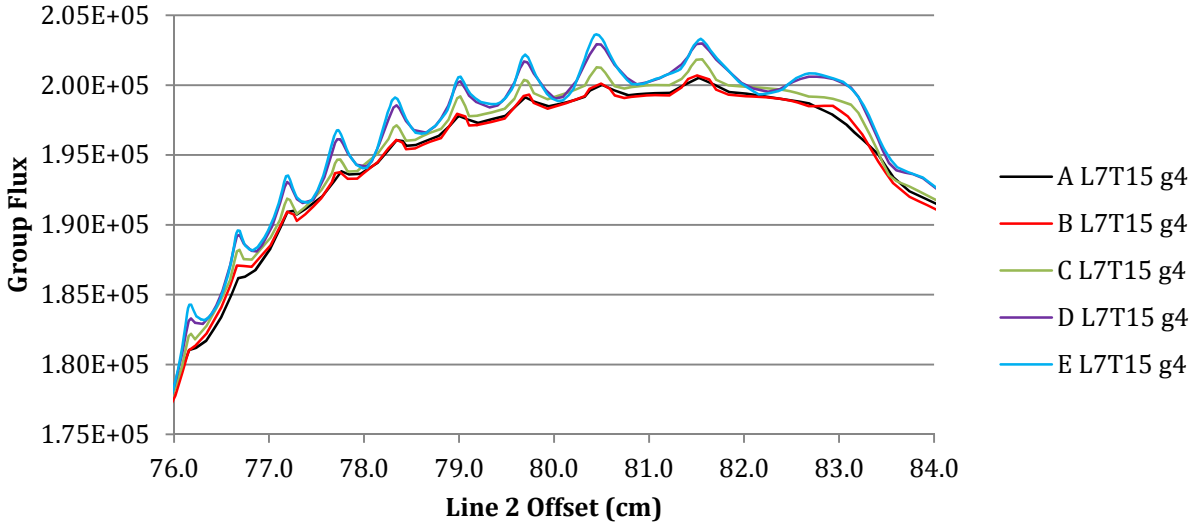

Figure 15. Close-up of Fast Flux Solution (Group 4) in Fuel Bundle for Line 1.

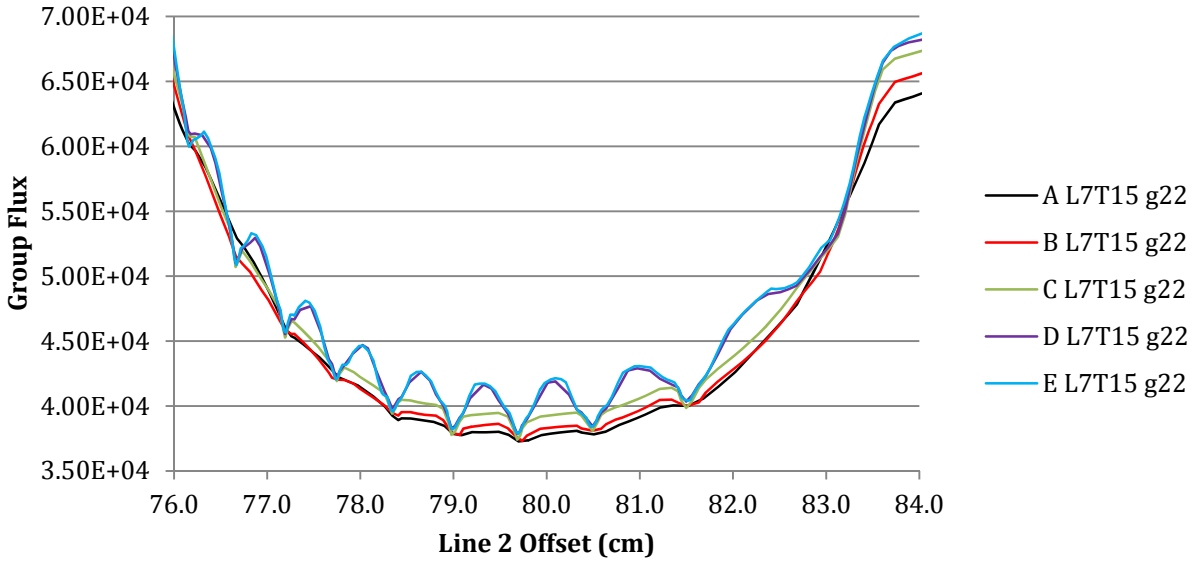

Figure 16. Close-up of Thermal Flux Solution (Group 22) in Fuel Bundle for Line 1.

In addition to convergence of the flux with respect to mesh, we must also consider convergence with respect to the angular cubature which is displayed here by fixing the mesh (Mesh D). Figure 17 displays the eigenvalue convergence with respect to angular cubature and clearly shows that the Tchebychev order is more important than the Legendre order for the eigenvalue. In this case, we ran additional Tchebychev orders to show the non-asymptotic convergence which is consistent with the complex geometry of the ATR and notably different than a conventional PWR or BWR calculation. From Figure 17, the eigenvalue appears to be reasonably converged using L3T11 (96 angles on the sphere) and L5T13 should be sufficient for most dynamics needs assuming a

different energy structure does not increase the angular cubature requirements (which should not happen in a thermal system like this).

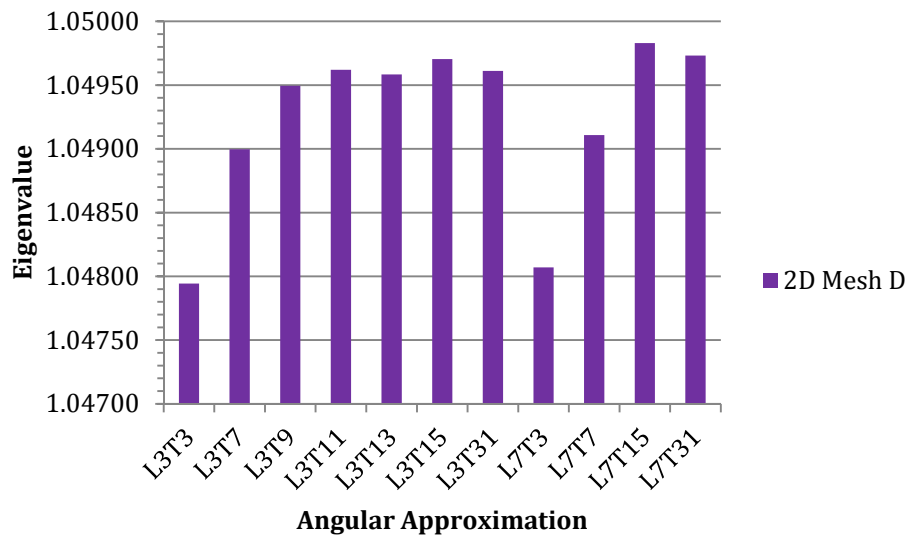

Figure 17. Angular Dependence of the Eigenvalue for Mesh D.

Flux convergence in the fuel bundle with respect to angular cubature is illustrated in Figure 18 and Figure 19 for Mesh D. These figures show a relatively smooth transition towards the final flux shape as the angular cubature is refined. We note that the fuel region is clearly inaccurate when using the coarser angular cubature settings (lack of peaks in the fast flux indicates a lack of accuracy in the within-group operator). Past the L3T11 cubature, changes in the flux solution are difficult to discern, which is consistent with the changes in the eigenvalue.

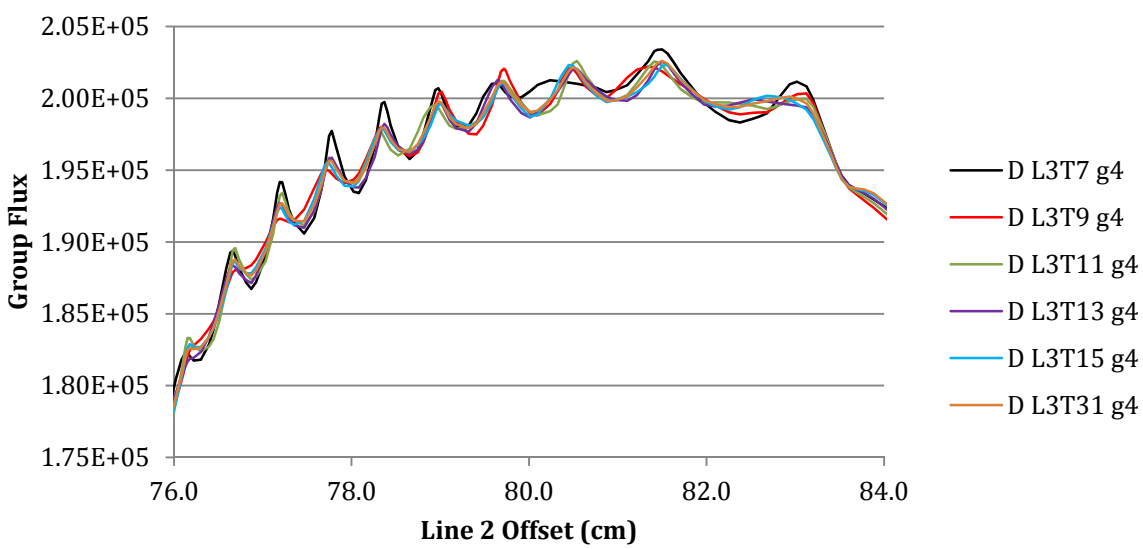

Figure 18. Mesh D, Fast Flux (Group 4) Solutions in a Fuel Bundle.

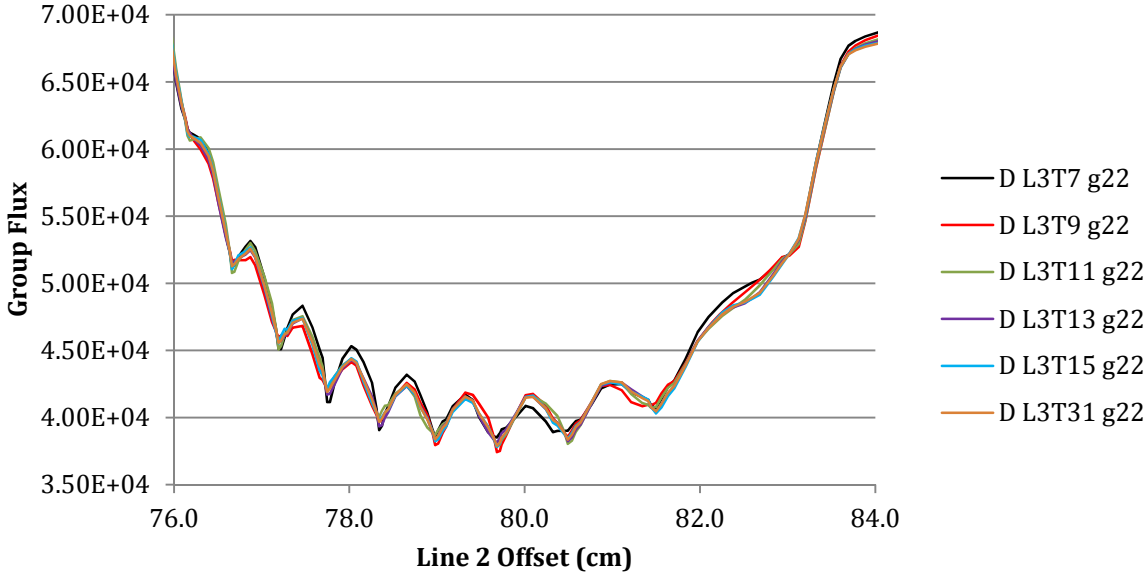

Figure 19. Mesh D, Thermal Flux (Group 22) Solutions in a Fuel Bundle.

In addition to the detailed study within a fuel bundle, the spatial mesh convergence was studied for the hafnium shim rods. As discussed previously, the primary changes in the mesh refinement in these regions were carried out between Mesh A and Mesh B where the sizes in Mesh B were maintained in meshes C through E. Figure 20 and Figure 21 show the Group 4 and Group 22 flux distributions in these hafnium regions where there are clearly six cylinders visible in the Group 22 flux solution; short stubby peaks correspond to the water region inside of each hafnium annulus while the higher flat top peaks are the water regions between the hafnium cylinders. Additional mesh refinement might be necessary between the hafnium cylinders due to the "blocky" nature of the solution (there is only a single element between these cylinders as seen in Figure 2 and Figure 4), but this will likely have a minor impact on the eigenvalue.

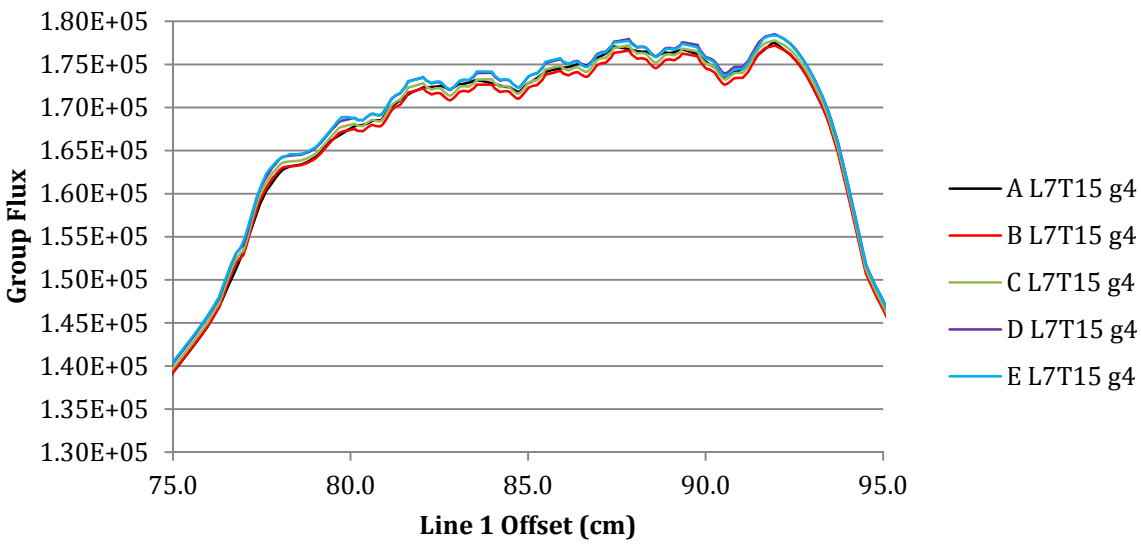

Figure 20. Fast Flux (Group 4) Solutions in the Central Hafnium Control Rod Regions.

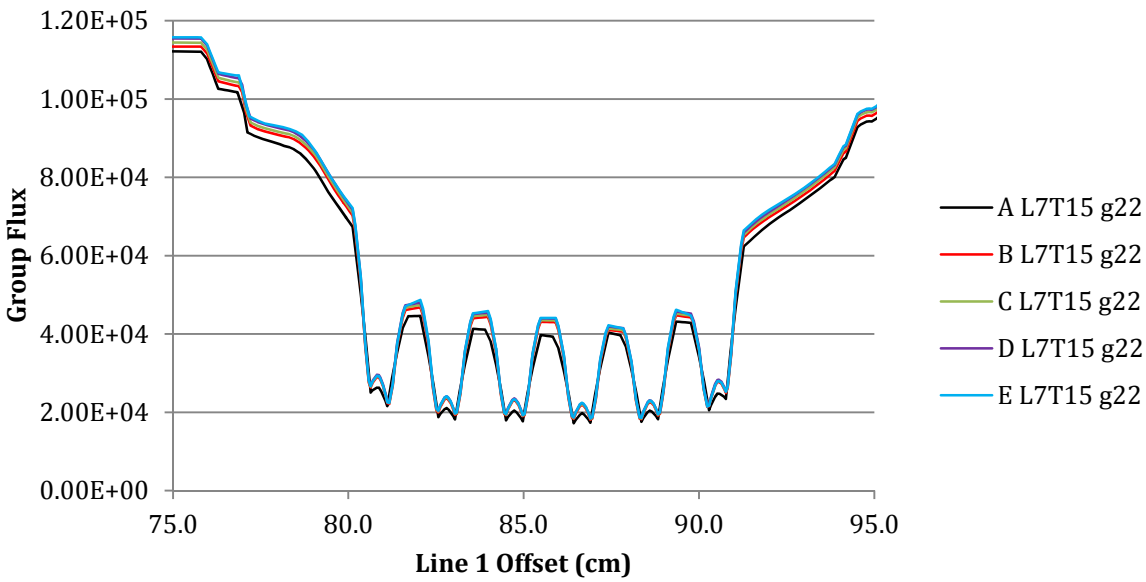

Figure 21. Thermal Flux (Group 22) flux in the Central Hafnium Control Rod Regions.

While the preceding analysis cannot be considered a complete confirmation of space-angle mesh refinement everywhere in the domain, experience with heterogeneous reactor problems and the SN2ND solver gives us enough confidence to say it is very close. In summary, the eigenvalue and flux solutions are found to converge sufficiently when using a L3T11 angular cubature (96 points on the sphere) and Mesh D (~260,000 linear elements). From the preceding, the fuel meat and water channels in each fuel bundle <u>must</u> be refined radially into a minimum of 3 elements each to preserve the local (flux) and global (eigenvalue) quantities using the SN2ND solver. Further, while lengthwise refinement is less important it must be fine enough to maintain well-conditioned elements in the fuel (especially if thermal mechanics is to be used). These characteristics should be consistent with any other transport solver

although local integral quantities can be comparably more accurate than SN2ND (i.e. a discontinuous finite element methodology). We also note that solution methodologies which incorporate higher order polynomial methodologies could require less mesh refinement as the observable gradients can be managed (the fuel meat is trivially thin and water channels are very narrow).

1.3 Spatial Convergence in 3D

The difference between 2D and 3D results should be dominated by the reflection in the regions adjacent to the active core. Consequently, the axial representation of the ATR was simplified to only capture the heterogeneity directly above and below the active core. This geometry was chosen in order to quickly produce a 3D model although a more complex geometry can be constructed as desired.

The 5 axial zones constructed for the 3D model are illustrated in Figure 22 whereas Figure 23 shows the detailed geometry model with exposed component pieces. Zone 3 is the centrally located 121.9 cm active core region. Zones 2 and 4 are 1.9 cm thick and are located directly below and above the active core where the fuel meat is replaced by an aluminum/water mixture. Zones 1 and 5 are the outer axial zones extending 19.05 cm below Zone 1 and 23.495 cm above Zone 5. In Zones 1 and 5, the fuel meat is replaced by a different aluminum/water mixture. Other than the fuel meat regions, all other materials from the two-dimensional geometry were simply extruded to the full height of 168.275 cm; the water channels, fuel cladding, beryllium, and hafnium. This is clearly a significant simplification of the real ATR geometry, but this model should provide a good estimate of the number of elements required in the axial reflector zones and the fuel region.

Two initial calculations, Model I and Model II, were performed using Mesh D extruded as described above. The axial meshing used for Model I and Model II are fully described in Table 3. As can be seen, in Model I, the fuel region is subdivided into equal intervals of ~6.8 cm while in Model II, the fuel region is subdivided into equal intervals of ~3.8 cm. Model I has a total of 6,912,135 vertices and 6,837,558 finite elements while Model II has a total of 11,264,220 vertices and 11,308,269 finite elements. Similar to the previous two-dimensional analysis, the flux solution was examined along a line extending vertically through fuel plate 16 in fuel bundle 1, termed "Line 3". It was found, as expected, that ~7 cm meshing within the central part of the fuel meat was more than adequate, but a more refined mesh is required in the axial zones close to the axial reflector regions. Model III was created to incorporate the finer meshing required near the active core boundaries where Table 4 lists the mesh details (note the 9.8 cm and 2.0 cm meshing in the active core region). Model III has a total of 9,728,190 vertices and 9,730,371 finite elements, which lies between that of Model I and Model II.

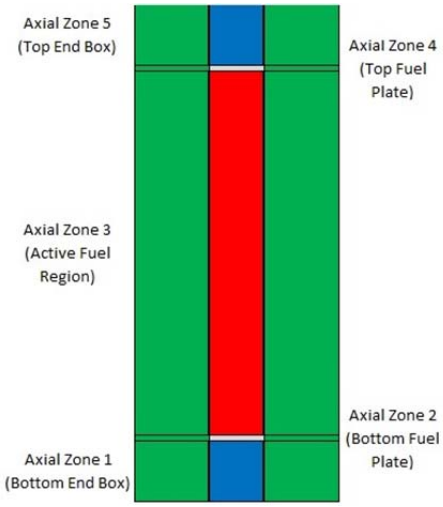

Figure 22. Simplified 3D Geometry (not to scale).

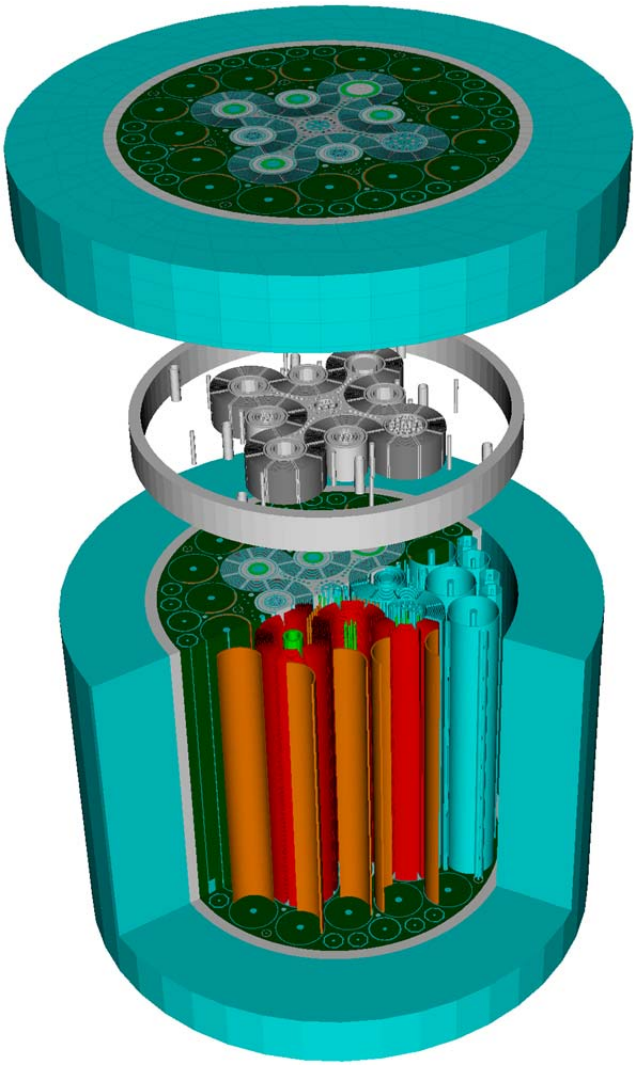

Figure 23. Detailed 3D Geometry of the ATR Calculations with Exposed Components.

Table 3. Axial Mesh Details for Model I and Model II.

Axial Zone	Description	Upper Z (cm)	Width (cm)	Model I Mesh		Model II Mesh	
				Axial Elements	Height (cm)	Axial Elements	Height (cm)
5	Top End Box	168.275	23.495	3	7.832	5	4.699
4	Top Fuel Plate	144.780	1.905	1	1.905	1	1.905
3	Active Fuel Region	142.875	121.920	18	6.773	30	4.064
2	Bottom Fuel Plate	20.955	1.905	1	1.905	1	1.905
1	Bottom End Box	19.050	19.050	3	6.350	5	3.810

Table 4. Axial Mesh Details for 3D Model III.

Axial Zone	Description	Upper Z (cm)	Width (cm)	Axial Elements	Height (cm)
5B	Top End Box - Upper	168.275	15.495	3	5.165
5A	Top End Box - Lower	152.780	8.000	4	2.000
4	Top Fuel Plate	144.780	1.905	1	1.905
3C	Active Fuel Region - Upper	142.875	12.000	6	2.000
3B	Active Fuel Region - Middle	130.875	97.920	10	9.792
3A	Active Fuel Region - Lower	32.955	12.000	6	2.000
2	Bottom Fuel Plate	20.955	1.905	1	1.905
1B	Bottom End Box - Upper	19.050	8.000	4	2.000
1A	Bottom End Box - Lower	11.050	11.050	2	5.525

The same energy groups used for the 2D study were chosen for the 3D calculation, and the flux plots are given in Figure 24 and Figure 25 where the L3T11 angular cubature was used. As can be seen, the Group 4 flux distribution is rather smooth, and one can expect the Model I mesh refinement to be sufficient. The same cannot be said of the Group 22 flux distribution where the water wings clearly require additional mesh refinement. While Model III is a significant improvement, especially noting the convergence in location of the flux depression at the end of the active core, it still requires refinement as evident from the fine point as opposed to smooth curve at the peak of the water wing. Such mesh refinement is rather easy to implement as desired in the future. Even with the relatively coarse nature of the flux solution in the axial water wings, the eigenvalue results in Table 5 are rather insensitive since a 47 pcm net change is observed from the clearly insufficient Model I mesh to the Model III mesh.

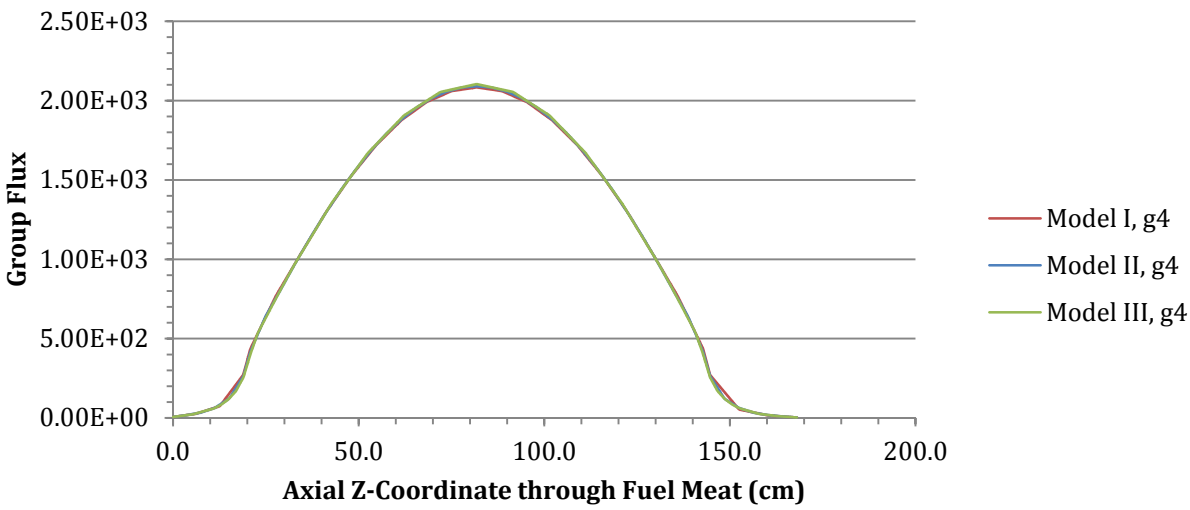

Figure 24. Fast Flux (Group 4) Solutions Along Line 3.

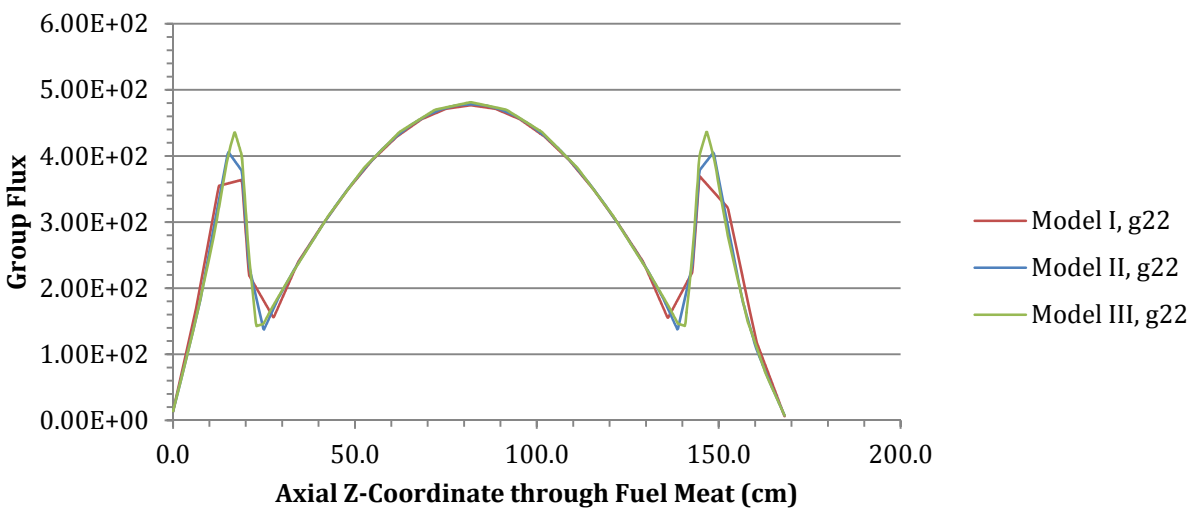

Figure 25. Thermal Flux (Group 22) Solutions Along Line 3.

Table 5. Eigenvalues from the 3D ATR Calculations.

3D Mesh	# Vertices	# Elements	Eigenvalue
Model I	6,912,135	6,837,558	1.02031
Model II	11,264,220	11,308,269	1.02017
Model III	9,728,190	9,730,371	1.01984

Figure 26 shows detailed 3D flux plots of both fast and thermal groups. In Figure 26, a section of fuel plates was separated to display the flux gradients on each plate along with various slices through the core centerline and upper core/reflector edge. The preceding 3D calculations show that fine (~2 cm) axial meshing is required in transition zones near the active fuel region boundaries, but coarse (~10cm) meshing is adequate

within the central part of the fuel. The number of vertices required to analyze a more accurate 3D geometry could be considerably reduced given the decreased geometrical detail above and below the active core, but that is rather difficult to achieve in conformal finite element meshing.

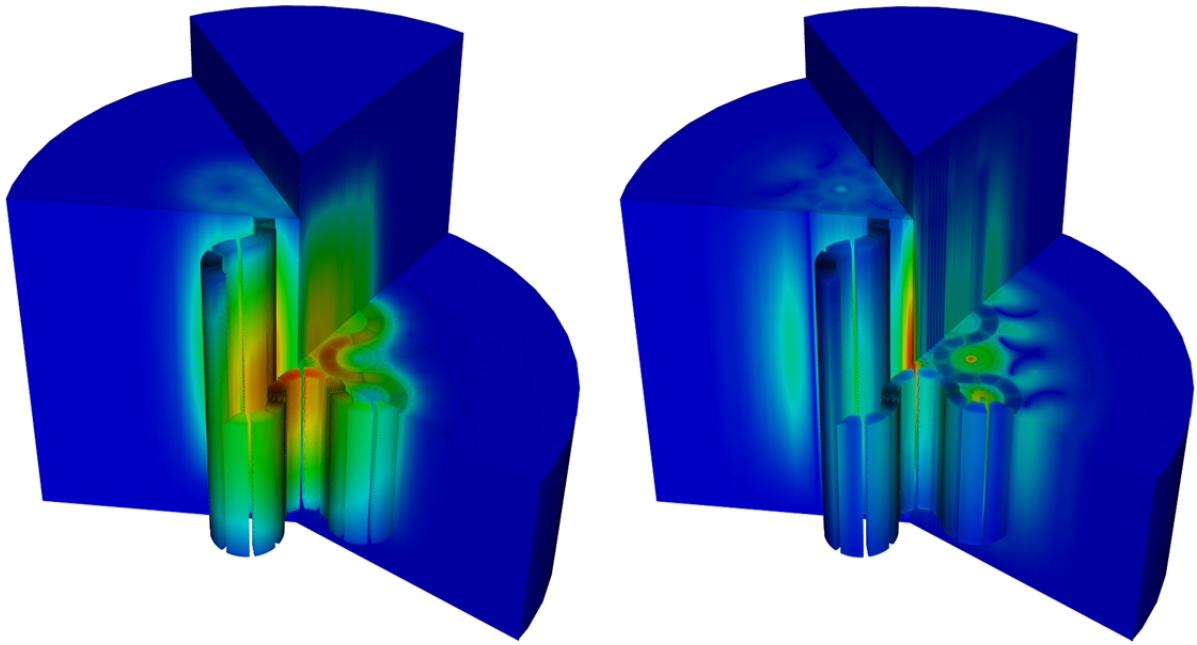

Figure 26. Fast (Group 4, Left) and Thermal Flux Plots (Group 22, Right).

1.4 Dependence on Cross Section Data

INL provided a SCALE input file for generating multi-group cross sections, which we modified to incorporate all materials in the geometry. Multigroup cross sections were generated for three energy group structures: 23g, 27g, and 49g. The definition of these group structures, as well as the 23g DRAGON structure, is given in the Appendix of this report. Note that the 23g DRAGON and 23g SCALE structures are similar, but not identical. Most notably, the SCALE group structures contain more energy groups in the lower thermal energies than the 23g DRAGON set which is consistent with the lower temperature of the ATR relative to a PWR.

The 2D Mesh D, L3T11 problem was performed using the four different cross section sets, and the eigenvalues are summarized in Table 6. As can be seen, there is significant disagreement between the different libraries which is clearly attributable to the different group structures and generation procedure (note that the 27 group library is meant for spent fuel casks). The use of anisotropic (P_1) scattering versus transport corrected isotropic scattering also yields the expected change, although we note that SCALE technically fitted the data using P5 and no BHS approximation was utilized. In this situation, we expect the use of the P_1 scattering data to result in an over-prediction of the leakage which was verified by performing a P_3 calculation with the SCALE 23g cross section which yielded an eigenvalue of 1.06337. Note that this is consistent when

using the P_1 scattering data from DRAGON, which cannot generate higher order scattering data.

Table 6. Eigenvalues from the 2D ATR Calculations with Different Cross Section Sets

Cross Section Set	P0 Scattering, Transport XS On	P1 Scattering, Transport XS Off
DRAGON 23g	1.04962	1.04650
SCALE 23g	1.06721	1.06080
SCALE 27g	1.05902	1.05322
SCALE 49g	1.06302	1.05714

Given that the ATR configuration used in all of these calculations is supposed to be critical, it should be clear that the preceding results leave much to be desired with regard to accuracy of the eigenvalue. While a few hundred pcm error is acceptable, the best the preceding results can offer is ~1.02 or 2000 pcm in error. As a consequence, any future analysis should involve significant effort devoted to the cross section generation process. We suggest implementing the sub-group method as a first step. In the end, the ATR presents significant issues for any conventional cross section generation procedure and it is very realistic to assume that more energy groups will be necessary to get the desired solution accuracy.

1.5 Computational Requirements

All of the preceding calculations were performed on Argonne's Leadership Computing Facilities [8], Challenger and Intrepid (IBM BG/P systems), using the SN2ND solver of UNIC.

A majority of the 23 group DRAGON 2D calculations took ~14 minutes where maximum parallelization in angle (1 angle per process) was combined with typical parallelization settings in space (1500-2000 vertices per process). In some cases, the number of angular directions did not yield ideal processor counts (i.e. multiples of 8) and thus the parallel setup was modified accordingly (e.g. the 2D Mesh D L3T11 case required ~17 minutes). With these basic settings we know that SN2ND is at the ~75% efficiency with respect to angle parallelization and 85% efficiency with respect to space (~60% efficiency overall). While we can choose to use 3000 vertices and 4 angles per process to get to +90% scaling, the ATR problem size does not require it at this time. Also note that the computational time would increase by a factor of ~8 and thus ~1.1 hours per steady state solve which is rather unrealistic for a dynamics simulation.

The problem size, and correspondingly, the computational requirements, increase dramatically when doing a 3D calculation due to the increased number of vertices, the individual element matrix sizes, and the number of connections per element. The 3D Model III case (L3T11, Mesh D with an optimized axial mesh) took ~80 minutes using 65,536 cores, 40% of the BlueGene/P supercomputer. In that calculation we used 16 angles per process and 2,375 vertices per process. A minimum of 1000 vertices per process must be used in the current SN2ND solver and 1 angle which means we can

achieve at best a factor of ~20 times improvement with a larger supercomputer (assumed 60% overall efficiency). Consequently, without further improvements in performance, a dynamics calculation with SN2ND is rather impractical at this time. While our recent research has indicated the proper steps required to achieve about an order of magnitude improvement in performance (along with several orders of magnitude in problem size), significant effort is required to implement such changes in addition to the work required to update the cross section treatment. As a final note, BlueGene/Q will be available soon which is expected to have a 4 times the number of cores, each of which is ~3 times faster than BlueGene/P, thereby mitigating the problems mentioned thus far. We do not presently have time on that machine due to preceding lack of support on INCITE proposals.

SUMMARY

The Advanced Test Reactor was analyzed using the SN2ND code, developed by Argonne National Laboratory under NEAMS. A space-angle convergence study was conducted to determine the meshing and angular cubature requirements for this problem, and also to demonstrate the feasibility of performing this analysis with a deterministic transport code capable of modeling heterogeneous geometries.

The work performed indicates that at a minimum, 2D spatial refinement on the order of 260,000 elements combined with a L3T11 cubature (96 angles on the sphere) are required for both eigenvalue and flux convergence. The fuel meat and water channels must each be meshed with at least 3 "radial zones" for accurate flux convergence. More studies are needed to determine the detailed flux convergence of the measurement zone regions, as this study focused on the eigenvalue and thus convergence of the flux near the fuel bundles.

A 23 group DRAGON cross section set was chosen because of its availability and used for a majority of the calculations. Near the end of this project, INL provided a SCALE input deck for generating ATR cross sections. A few select 2D calculations were performed using 23 group, 27 group, and 49 group data generated from SCALE which did not have a major impact with respect to accuracy (~1100 pcm higher than the DRAGON based results which were expected to be terribly incorrect). The fact that the ATR configuration modeled in this work was approximately critical and the best any of the multi-group libraries could infer was an eigenvalue of ~1.02, one should invest more effort into the multi-group cross section generation process.

The total number of degrees of freedom for a converged 27 group, 2D problem is ~340 million (27g x 48 angles x 260,000 vertices). The corresponding number of degrees of freedom for a fully converged 3D calculation with the same number of energy groups is ~25 billion (27 g x 96 angles x 9.7 million vertices). Such calculations are well within the capabilities of the current SN2ND solver which has been used on upwards of 500 billion degrees of freedom, but dynamics calculations are unlikely without the stated improvements in the solver or computer resources. In any case, fully 3D dynamics calculations cannot be performed efficiently on a single workstation and

require a large scale computing center which we estimate to be ~2,048 processes for 2D problems and ~65,000 processes for a 3D problem using the existing SN2ND solver.

ACKNOWLEDGMENTS

The calculations in this report were performed with SN2ND, a parallel neutronics solver developed by Argonne National Laboratory under the NEAMS program. This research used resources of the Argonne Leadership Computing Facility at Argonne National Laboratory, which is supported by the Office of Science of the U.S. Department of Energy under contract DE-AC02-06CH11357.

REFERENCES

1. S.S. Kim, et al., "Advanced Test Reactor: Serpentine Arrangement of Highly Enriched Water-Moderated Uranium-Aluminide Fuel Plates Reflected by Beryllium." NEA/NSC/DOC(95)-03/II, HEU-MET-THERM-22. Idaho National Laboratory, 2005.
2. Micheal A. Smith, Dinesh Kaushik, Allan Wollaber, Won Sik Yang, Barry Smith, Cristian Rabiti, Giuseppe Palmiotti, "Recent Research Progress on UNIC at Argonne National Laboratory," Proc. International Conference on Mathematics, Computational Methods & Reactor Physics, Saratoga Springs, New York, May 3-7, 2009.
3. A. Siegel, T. Tautges, A. Caceres, D. Kaushik, and P. Fischer, "Software Design of SHARP," Proc. Joint Int'l Topical Mtg. on Mathematics & Computation and Supercomputing in Nuclear Applications, Monterey, California, April 15–19, 2007.
4. D. Kaushik, M. A. Smith, A. Wollaber, B. Smith, A. Siegel, W. S. Yang, "Enabling High-Fidelity Neutron Transport Simulations on Petascale Architectures," Proc. International Conference for High Performance Computing, Networking, Storage and Analysis, Portland, Or, November 14-20, 2009.
5. Vijay S. Mahadevan, Michael A. Smith, "Scalable Multi-grid Preconditioning techniques for the even-parity SN solver in UNIC," International Conference on Advances in Mathematics, Computational Methods, and Reactor Physics (M&C), Rio de Janeiro, Brazil, in May 8-12, 2011.
6. M. A. Smith, A. Mohamed, C. H. Lee, A. Marin-Lafleche, and W. S. Yang, "Zero Power Fast Reactor Deterministic Modeling with Heterogeneous Geometry," American Nuclear Society, Hollywood, FL, June 26-30, 2011.
7. A. Mohamed, W. S. Yang, M. A. Smith, and C. H. Lee, "Spectrum Interaction Effects on Calculating Foil Reaction Rates in ZPR Assemblies," International Conference on Advances in Mathematics, Computational Methods, and Reactor Physics (M&C), Rio de Janeiro, Brazil, in May 8-12, 2011.

8. Argonne National Laboratory, Argonne Leadership Comp. Facility, http://www.alcf.anl.gov.
9. Marleau, G., A. Hébert, R. Roy, A User's Guide for DRAGON, Ecole Polytechnique de Montréal, December 1997.
10. *SCALE: A Comprehensive Modeling and Simulation Suite for Nuclear Safety Analysis and Design*, ORNL/TM-2005/39, Version 6.1, Oak Ridge National Laboratory, Oak Ridge, Tennessee, June 2011. Available from Radiation Safety Information Computational Center at Oak Ridge National Laboratory as CCC-785.
11. T. D. Blacker, et al.,"CUBIT mesh generation environment. Volume 1: Users manual," SAND--94-1100, Sandia National Laboratory, 1994.

APPENDIX

Table A1. Energy Group Structures Used in this Report (the lowest energy for all structures is 10^{-5} eV).

Group Number	SCALE 49g Upper Energy (eV)	SCALE 27g Upper Energy (eV)	SCALE 23g Upper Energy (eV)	DRAGON 23g Upper Energy (eV)
1	2.00E+07	2.00E+07	2.00E+07	1.00E+07
2	8.19E+06	6.38E+06	4.80E+06	3.68E+06
3	6.43E+06	3.01E+06	1.40E+06	1.35E+06
4	4.80E+06	1.83E+06	5.50E+05	5.00E+05
5	3.00E+06	1.42E+06	1.28E+05	1.11E+05
6	2.48E+06	9.07E+05	7.50E+04	6.73E+04
7	2.35E+06	4.08E+05	1.30E+04	9.12E+03
8	1.85E+06	1.11E+05	6.70E+02	3.67E+02
9	1.40E+06	1.50E+04	4.75E+00	4.00E+00
10	9.00E+05	3.04E+03	1.59E+00	1.50E+00
11	4.00E+05	5.83E+02	1.11E+00	1.10E+00
12	1.00E+05	1.01E+02	1.06E+00	1.05E+00
13	2.50E+04	2.90E+01	1.00E+00	9.72E-01
14	1.70E+04	1.07E+01	9.00E-01	8.50E-01
15	3.00E+03	3.06E+00	5.50E-01	5.00E-01
16	5.50E+02	1.86E+00	4.50E-01	4.00E-01
17	1.00E+02	1.30E+00	3.75E-01	3.50E-01
18	3.00E+01	1.13E+00	3.25E-01	3.00E-01
19	1.00E+01	1.00E+00	2.75E-01	2.50E-01
20	8.10E+00	8.00E-01	2.25E-01	1.80E-01
21	6.00E+00	4.14E-01	1.75E-01	1.40E-01
22	4.75E+00	3.25E-01	1.25E-01	1.00E-01
23	3.00E+00	2.25E-01	6.00E-02	5.00E-02
24	1.77E+00	1.00E-01		
25	1.50E+00	5.00E-02		
26	1.25E+00	3.00E-02		
27	1.15E+00	1.00E-02		
28	1.10E+00			
29	1.05E+00			
30	1.00E+00			
31	6.25E-01			
32	4.00E-01			
33	3.75E-01			
34	3.50E-01			
35	3.25E-01			
36	2.75E-01			

Group Number	SCALE 49g Upper Energy (eV)	SCALE 27g Upper Energy (eV)	SCALE 23g Upper Energy (eV)	DRAGON 23g Upper Energy (eV)
37	2.50E-01			
38	2.25E-01			
39	2.00E-01			
40	1.50E-01			
41	1.00E-01			
42	7.00E-02			
43	5.00E-02			
44	4.00E-02			
45	3.00E-02			
46	2.53E-02			
47	1.00E-02			
48	7.50E-03			
49	3.00E-03			

Nuclear Engineering Division
Argonne National Laboratory
9700 South Cass Avenue
Argonne, IL 60439

www.anl.gov

A U.S. Department of Energy laboratory
managed by UChicago Argonne, LLC